Electronic Supplementary Material (ESI) for Journal of Analytical Atomic Spectrometry

Depth dependent element ratios in fluid inclusion analysis by laser ablation ICP-MS

Marcel Guillong,*[a] and Thomas Pettke[b]

Instrumentation parameters:

Table ESI 1: Instrument parameters

Laser Ablation System	**Resonetics M50 HR**	
Laser and wavelength	193 nm ArF excimer (Compex pro 110)	
Energy density	0-30 J cm^{-2} (~ **15 J cm^{-2}**)	
Demagnification	15x, 20x, 25x, 30x, **35x**	
Crater size (35x demagnification)	5, 7, 9, **14, 19, 29, 34, 47, 64, 89**, 120, 163 ≅m	
Beam	non-homogenized	
Ablation Cell	Laurin Technic two-volume cell	
Aerosol mixing device	Squid	
He flow	0.6 l min^{-1}	
Software	Geostar 6.20	
ICP-MS	**Agilent 7500 cs/ce**	
Lens system	cs (nov.30)	ce (ja. 20)
RF Power	1380 W	1550 W
Make up gas flow (Ar)	0.86 l min^{-1}	0.88 l min^{-1}
sampling depth	3.9 mm	3.8 mm
Extraction lens 1 voltage	4.9 V	0 V
extraction lens 2 voltage	- 30 V	- 100 V
Omega bias -cs	-38 V	-22 V
Omega lens -cs	7.8 V	-2.4V
Cell entrance	-32 V	-36 V
QP focus	4 V	2 V
Cell Exit	-32 V	-50 V
QP Bias	-3 V	-3.5 V
Background mass 220	~ 3 cps	~ 0.7 cps
Background mass 23	~ 7000 cps	~ 75000 cps
Sensitivity U 238 *	~ 100000 cps	~ 48000 cps
Sensitivity Li 7 *	~ 20000 cps	~ 15000 cps
Oxides (ThO/Th) *	0.254%	0.228%
Doubely charged (22/44) *	0.048%	0.275%
U/Th *	1.16	1.21
cooling gas flow	15 l min^{-1}	
plasma gas flow	1.0 l min^{-1}	
reaction cell mode	no gas	
Octopole RF	200 V	
Octopole Bias	-17 V	
* NIST 612, 47 ≅m, 10 Hz, 3.5 J cm^{-2}, 3 ≅m s^{-1} scan		

Electronic Supplementary Material (ESI) for Journal of Analytical Atomic Spectrometry

Images of Fluid Inclusion assamblages:

Sample 208-37

Figures ESI 1 to ESI 4 show the fluid inclusion assemblage in sample 208-37: Figure ESI 1 shows an overview of a free standing quartz crystal with well visible growth zones with a magnification of the analysed assemblage that is on an inclined plane relative to the surface of the thick section. This represents a typical late pseudosecondary or secondary fluid inclusion assemblage located on a healed fracture. The inclination of the plane is well suited to explore depth-dependent features of inclusion analysis. Figure ESI 2 and ESI 3 show a series of microscope pictures of the assemblage at different focal planes. Figure ESI-4 shows an image taken with the CCD camera of the laser ablation system after ablation of the inclusions. Due to surface contamination inclusions remain hardly visible.

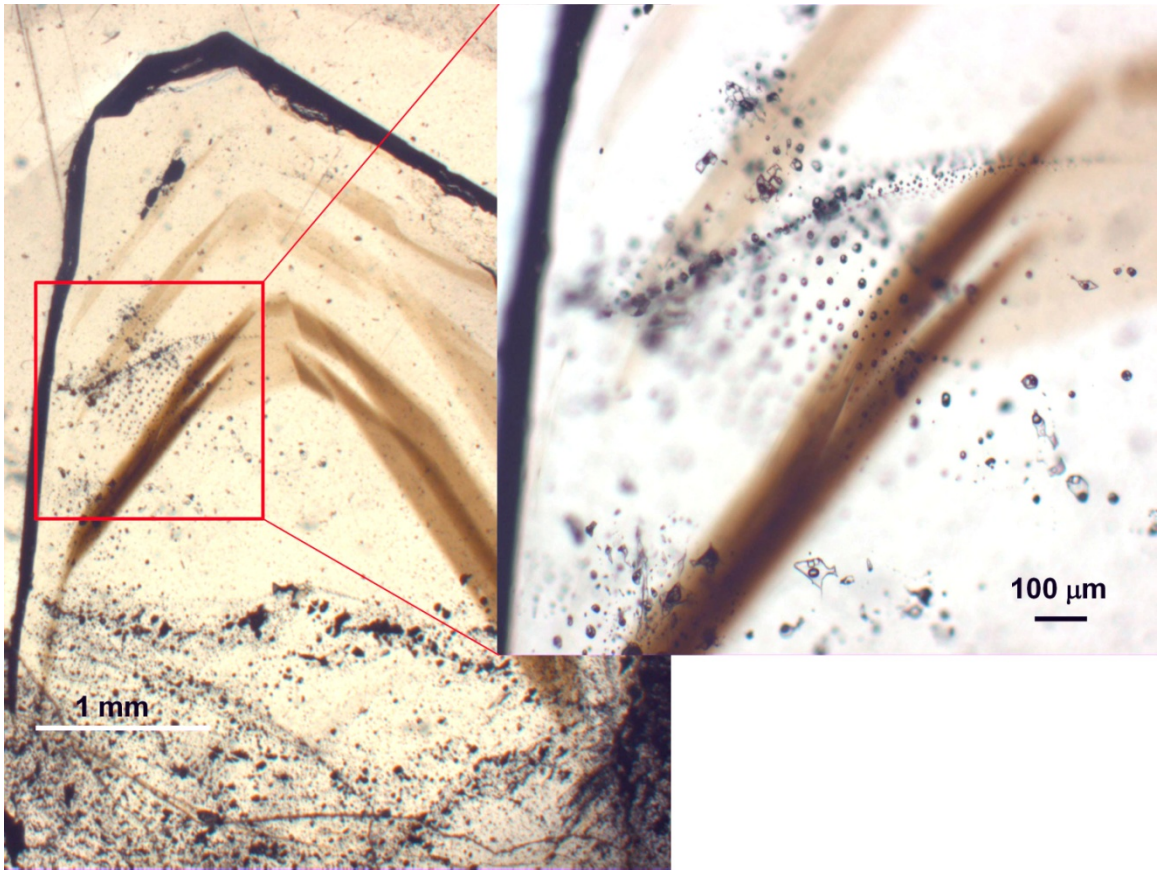

Figure ESI 1. Microscope pictures of sample 208-37 with the analysed inclusion assemblage.

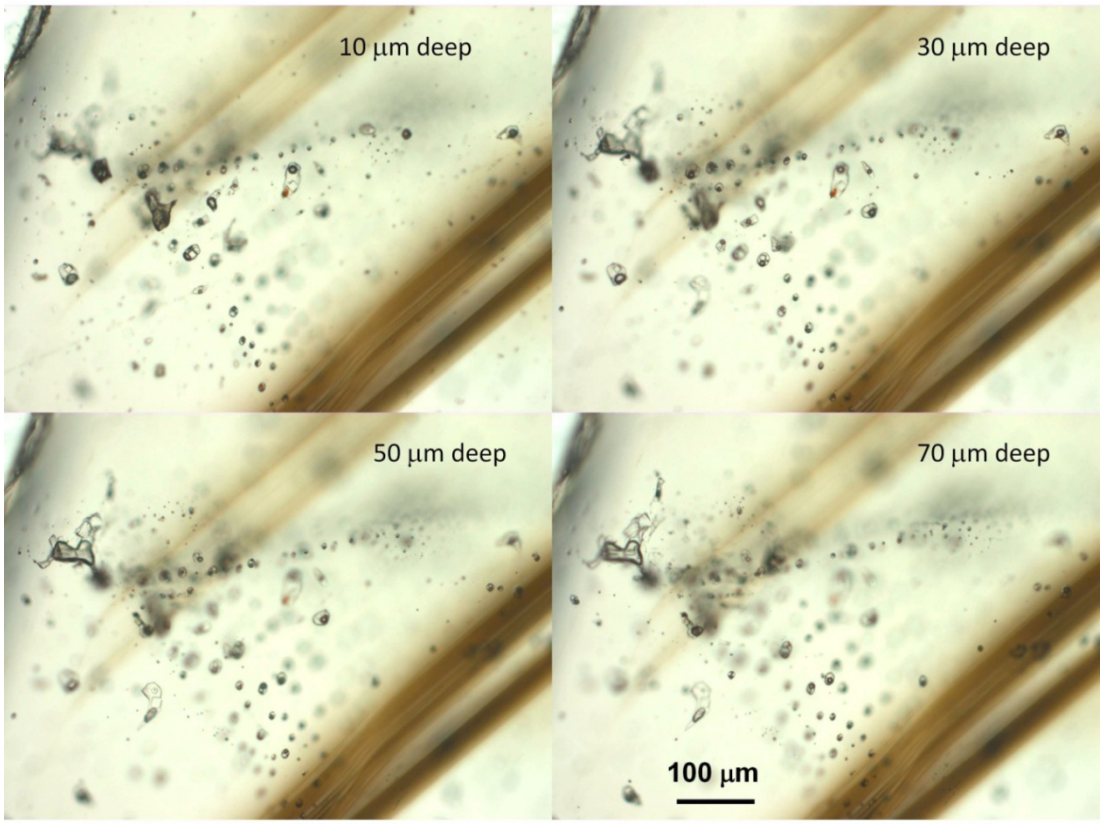

Figure ESI 2. Microscope pictures of inclusion assemblage sample 208-37 at different focal planes.

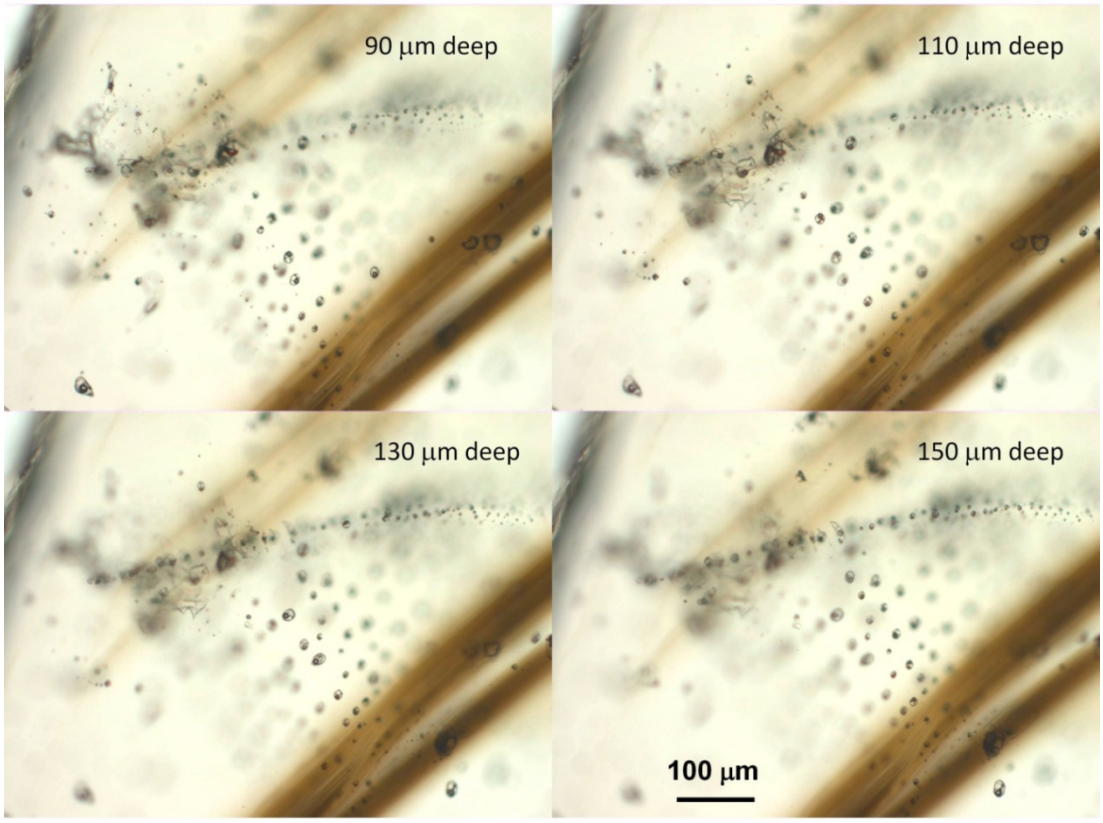

Figure ESI-3. Microscope pictures of inclusion assemblage sample 208-37 at different focal planes.

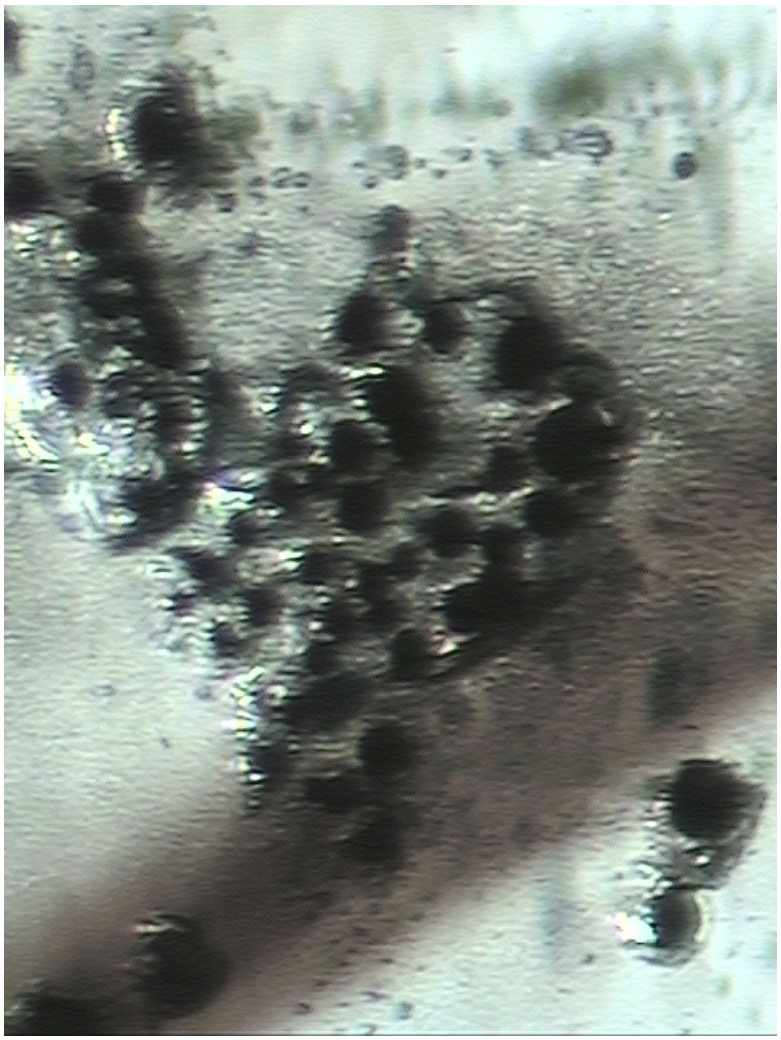

Figure ESI-4. CCD pictures of analysed inclusion assemblage sample 208-37 from the laser ablation system. Note the extensive surface contamination (deposited material) from the ablations, visible as relief texture around the craters.

Sample Loww9

Figure ESI 5 shows the inclusion assemblage of the Loww9 sample. The sample hosts pseudosecondary inclusion trails with 30-50 micron sized, well separated brine inclusions. Figure ESI 5 shows a comparison between an optical microscope and the Resonetics M50 visualization employing identical scales. The overview consists of merged individual images. The magnified areas show that the resolution is sufficient with M50 system to clearly identify and separate individual inclusions. Note that the depth of view is few tens of micrometers with the optical microscope and hundreds of micrometers with the M50 system. This can be problematic for visualization when many features are within and on the sample such as multiple inclusions or surface contamination (Figure ESI 4).

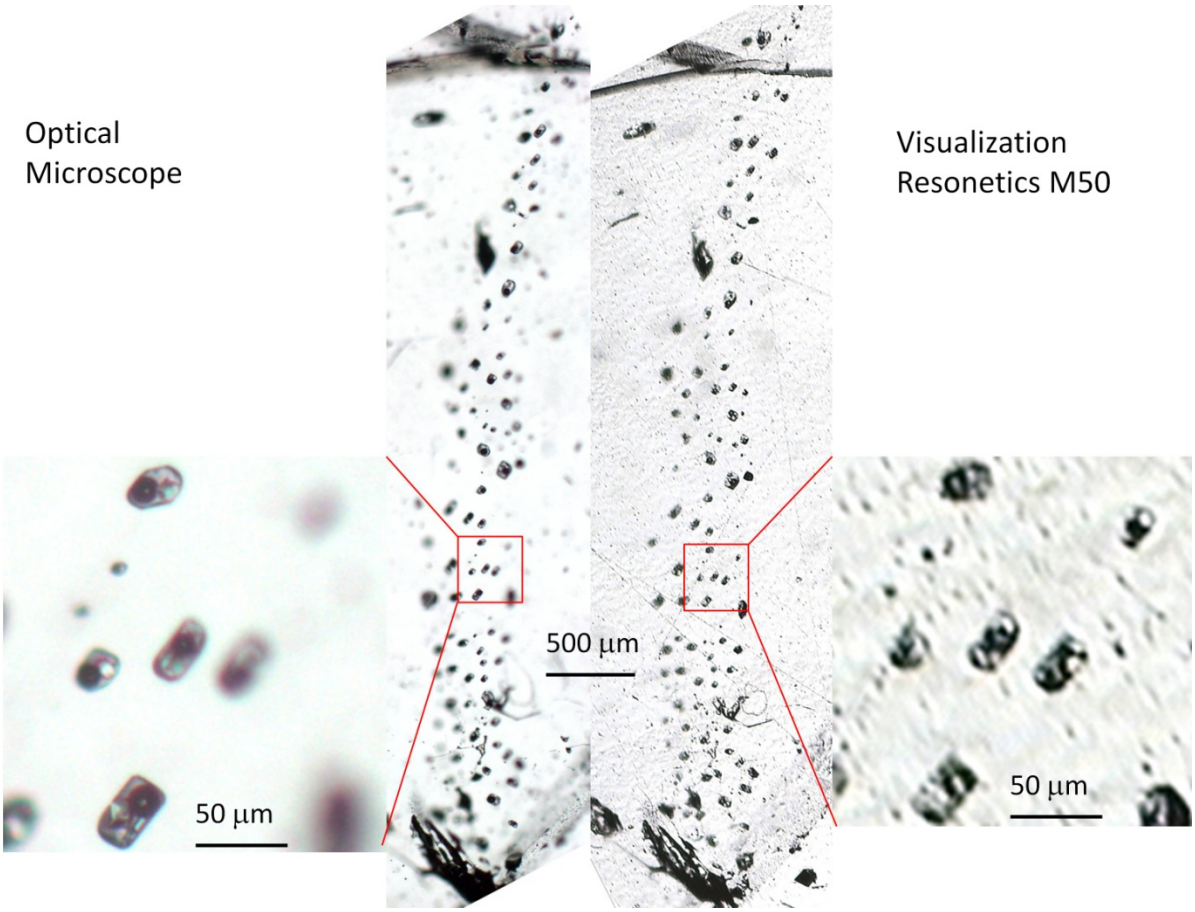

Figure ESI 5. Microscope (left) and ablation system CCD camera (right) pictures of the inclusion assemblage selected for analysis in sample Loww9. The enlarged views compare the same detail image for the two visualization systems.

Description of depth measurements:

Method 1: Microscopy prior to ablation

On an optical microscope (20 x magnifications) the surface above the inclusion was focused, and the value on the fine focusing knob was noted. After focusing on the circumference of the inclusion, the value of the fine focusing knob was noted again, the difference was calculated. The refractive index of this quartz sample was calculated based on the thickness of the quartz chip, measured with a Digital calliper to be 680 micrometer (Loww9). The optical microscope was then focused again on the surface of the chip and on the plane between the quartz chip and the microscope slide. This measurement resulted in 440 µm. The ratio is 1.545, close to the literature value for fused silica of 1.556 as calculated for 532nm on http://refractiveindex.info, respectively, while the values for quartz vary from 1.5442 to 1.5533, depending on crystal orientation. The measured differences of the microscope were then multiplied with the refractive index to get the real mean depth of the fluid inclusions.

Method 2: After laser ablation

The ablation rate was calculated based on the thickness of the quartz chip (Loww9) and an ablation through the quartz chip. 252 seconds at 10 Hz repetition rate and ~15 J/cm^2 energy density where necessary to drill through which corresponds to an ablation rate of 2.7 µm per second or 270 nm per pulse, in good agreement with previously published ablation rates for fused silica (e.g. 0.3 µm/pulse at 12 J/cm^2)[1, 2]. From the recorded transient signal of the fluid inclusion excavation it is possible to calculate the ablation time until the inclusion signal starts. Based on the ablation rate and the time until the inclusion signal starts, the minimal inclusion depth can be calculated.

Comparison of the two methods to calculate the depth of an inclusion:

Figure ESI 6 shows the correlation between the two measured depths: There is an acceptable correlation, with two obvious effects: Nominally, the difference between the two measurements is approximately ½ of the fluid inclusion size as the method 2 returns the minimal depth of the inclusion compared to a mean depth by method 1. Therefore, the trend of measurements cuts the x axis (method 1) at about 30 µm. Additionally, towards deeper inclusions, method 2 overestimates the depth. This might be due to a non linear ablation rate (decrease for craters deeper 300 microns)

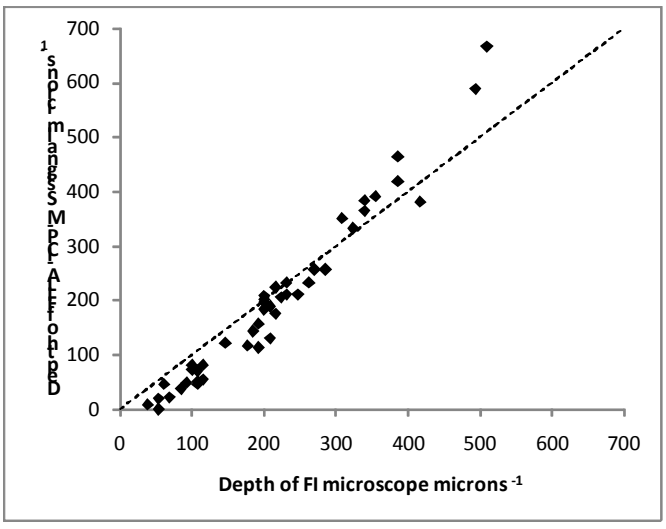

Figure ESI 6. Correlation between different depth measurements of fluid inclusions.

Electronic Supplementary Material (ESI) for Journal of Analytical Atomic Spectrometry

Description of measurement strategy for fluid inclusion analysis using a Resonetics M50 laser Ablation system equipped with the Geostar software:

1. **Sample holder scan:**
   A High resolution scan of the whole sample holder is coordinated with the stage for easy orientation of the laser within the cell and samples. Figure ESI 7 shows an example with the thin section (sample 208-37 on the left and a SRM mount on the bottom right, including NIST 610, NIST 612, Sca_17, BCR-2 G, GSD-1 G, and others). Note that the thick section has to be flat and the surface needs to be at a specific height in the sample holder.

2. **Keep images from the M50 CCD camera**
   Move the stage to the inclusions and keep images from the CCD camera, when the inclusions of interest are visible (transmitted light) and can be allocated with sample preparation figures. Figure ESI 8 shows a magnified part of ESI 7 within the Geostar software (saved display) with the kept images, as well as the yellow square indicating the actual location of the stage, visible on the live screen. With Geostar software it is possible to load and coordinate images from other sources like optical microscopes or electron microscope. This could be a possibility to locate inclusions that are poorly visible with the M50 optics. However this possibility was not explored in detail as it was possible in these samples to easily locate the inclusions.

3. **Mark all inclusions of interest**
   In figure ESI 9, all inclusions are marked at their locations for later reference, representing a sequence of single spots in the Geostar software. Although this feature of the software is not used for fluid inclusion analysis it is very helpful at a later stage, when the inclusions are not visible anymore due to surface contamination of previous ablations (see figure ESI 4). With Geostar software it is possible to import sample locations from other sources (e.g., computerized microscope stage or electron microscope) and coordinate them. However this possibility was not explored in this study.

4. **Analysis of SRM and inclusions**
   Now the system is ready for inclusion analysis. For the analysis we used the system manually. For a rapid crater change, the beam stop (shutter) can be opened and closed by a keyboard short cut, while the crater size is changed from the software graphical interface. Care has to be taken to not open the beam stop before the aperture wheel stopped rotating. If the surface contamination is too excessive (either for the recorded signal or visualisation) the sample can be taken out of the cell, repolished and put back, as shown in figure ESI 10.

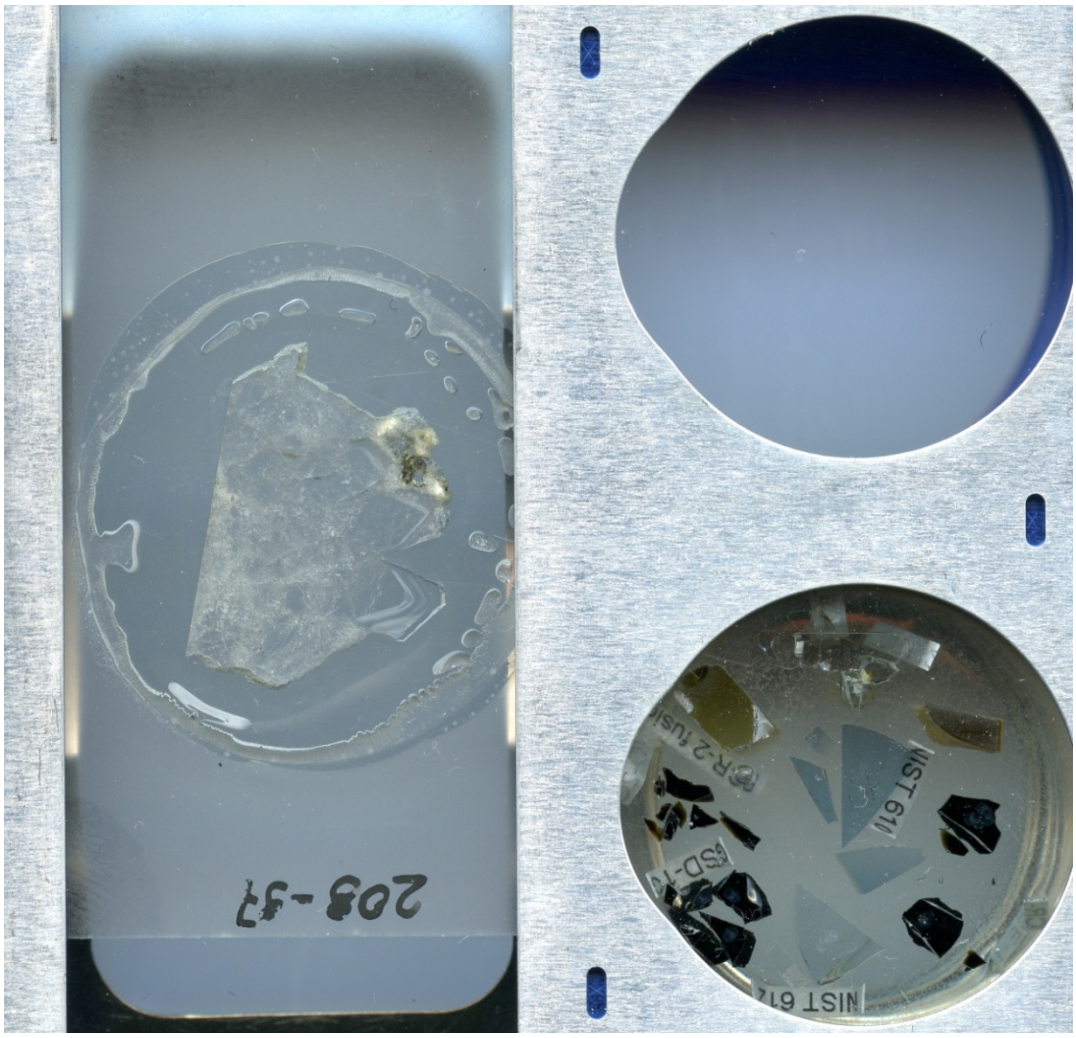

Figure ESI 7. Scanned image of sample holder with fluid inclusion sample 208-37 and SRM block.

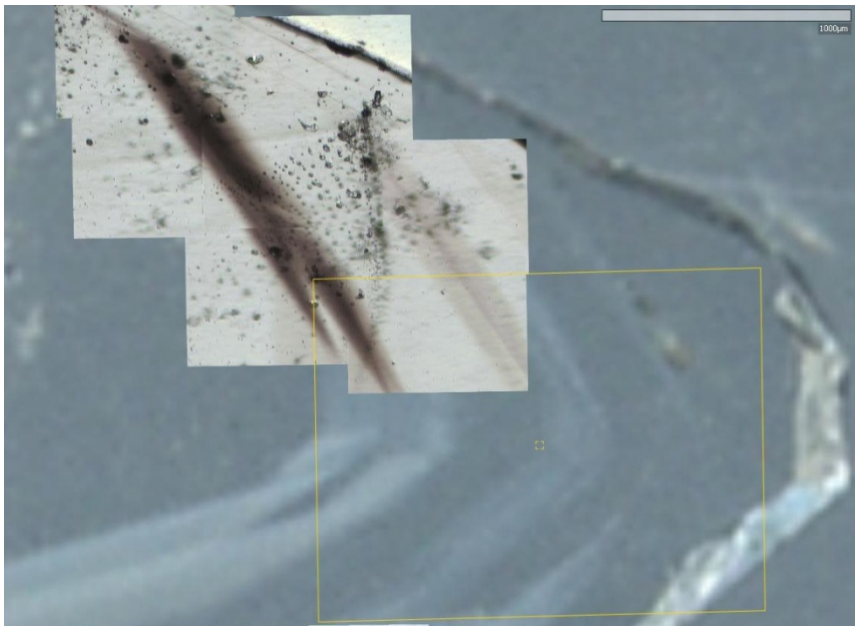

Figure ESI 8. Overlaid CCD camera images over the coordinated scan (Figure ESI 7) from the Geostar screen.

Figure ESI 9. Marked inclusions on CCD camera images on sample Loww9 from the Geostar software, each tagged with the analysis number.

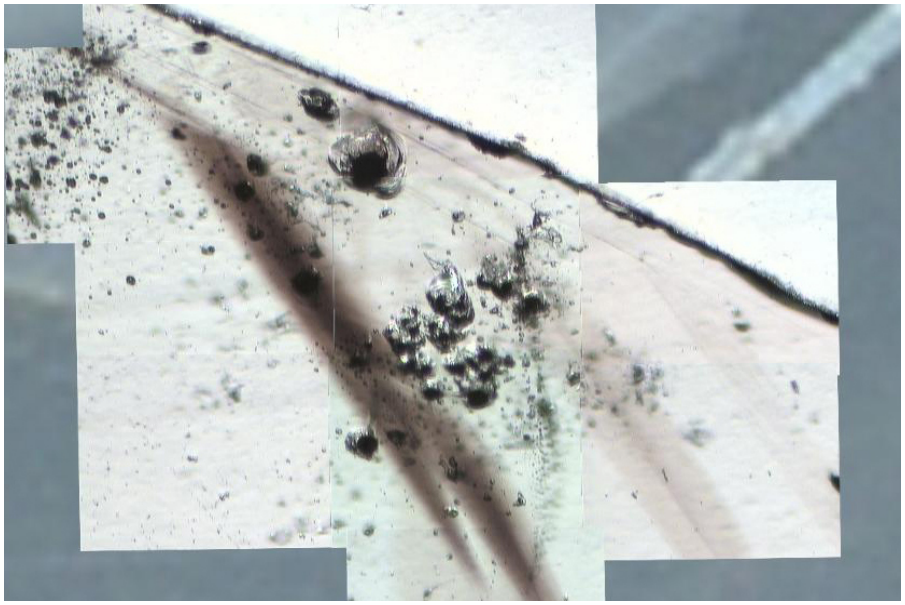

Figure ESI 10. Overlaid images after ablation and polishing to remove surface contamination (deposited material) from sample 208-37. The sample is now ready for the next series of inclusion analysis.

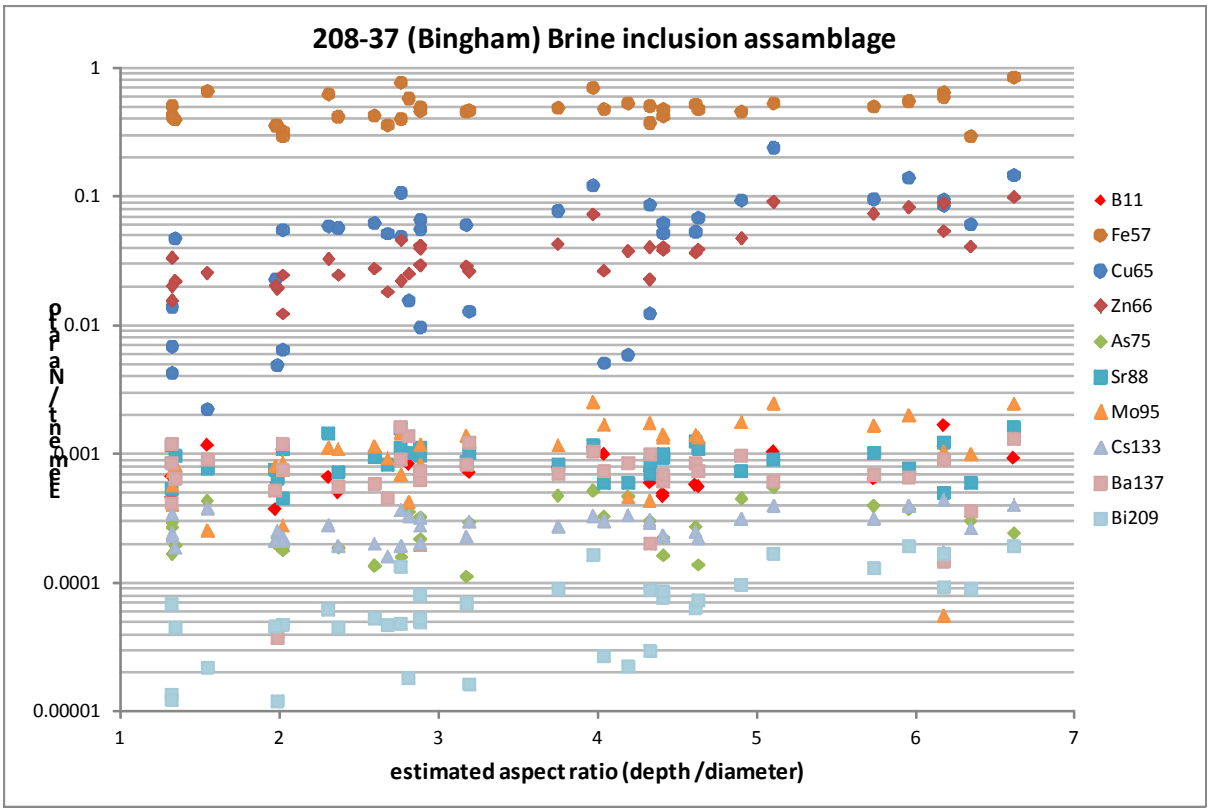

Figure ESI 11 Aspect ratio dependent element abundance ratios for individual brine inclusions from one late-entrapped assemblage of sample 208-37, Bingham canyon porphyry Cu-Au±Mo ore deposit. Data for elements not shown in figure 4.

Table ESI 2: Element concentration ratios relative to Na for all analysed inclusions (normalized to 45 wt-% NaCl equivalent), without obvious outliers due to incomplete sampling.

			Element To Na concentration ratios for individual fluid inclusions sorted by aspect ratio														
analysis name	Inclusion name	Aspect ratio	B11	Cl35	K39	Mn55	Fe57	Cu65	Zn66	As75	Rb85	Sr88	Mo95	Cs133	Ba137	Pb208	Bi209
nv30b09.csv	208-37_FI-7	1.32	0.0005	1.6	0.47	0.019	0.42	0.014	0.016	0.00017	0.17	0.12	0.0007	0.00024	0.0008	0.018	0.00001
nv30b13.csv	208-37_FI-16	1.32	0.0007	1.8	0.61	0.024	0.50	0.004	0.020	0.00029	0.21	0.05	0.0004	0.00034	0.0012	0.023	0.00001
nv30b13.csv	208-37_FI-16.1	1.32	bdl	1.8	0.54	0.024	0.43	0.007	0.033	0.00027	0.16	0.09	0.0006	0.00023	0.0004	0.034	0.00007
nv30a06.csv	208-37_FI-3	1.34	0.0006	1.7	0.39	0.021	0.40	0.047	0.022	0.00020	0.15	0.10	0.0008	0.00019	0.0006	0.025	0.00004
nv30b12.csv	208-37_FI-13	1.54	0.0012	1.9	0.56	0.030	0.66	0.002	0.026	0.00043	0.26	0.08	0.0003	0.00038	0.0009	0.025	0.00002
nv30b08.csv	208-37_FI-4	1.97	0.0004	1.5	0.41	0.019	0.36	0.023	0.020	0.00020	0.15	0.08	0.0008	0.00021	0.0005	0.025	0.00005
nv30a11.csv	208-37_FI-15	1.99	0.0006	1.8	0.38	0.022	0.36	0.005	0.019	0.00022	0.17	0.07	0.0002	0.00025	0.0000	0.017	0.00001
nv30a10.csv	208-37_FI-12	2.02	0.0002	1.8	0.42	0.022	0.32	0.055	0.025	0.00019	0.17	0.11	0.0009	0.00023	0.0008	0.028	0.00005
nv30b11.csv	208-37_FI-11	2.02	0.0011	1.3	0.37	0.016	0.29	0.006	0.012	0.00018	0.14	0.05	0.0003	0.00021	0.0012	0.016	0.00001
nv30a12.csv	208-37_FI-17	2.31	0.0007	2.0	0.66	0.031	0.62	0.059	0.033	bdl	0.17	0.15	0.0011	0.00028	bdl	0.035	0.00006
nv30a14.csv	208-37_FI-21	2.37	0.0005	1.7	0.38	0.022	0.42	0.057	0.025	0.00019	0.06	0.07	0.0011	0.00019	0.0006	0.026	0.00004
nv30a09.csv	208-37_FI-10	2.60	bdl	1.8	0.38	0.022	0.42	0.062	0.028	0.00014	0.15	0.09	0.0011	0.00020	0.0006	0.030	0.00005
nv30a08.csv	208-37_FI-8	2.68	bdl	1.7	0.36	0.018	0.36	0.052	0.018	bdl	0.12	0.08	0.0009	0.00016	0.0005	0.024	0.00005
nv30b10.csv	208-37_FI-9	2.76	bdl	1.3	0.34	0.022	0.40	0.049	0.022	0.00016	0.13	0.11	0.0007	0.00019	0.0009	0.026	0.00005
nv30b15.csv	208-37_FI-20	2.76	bdl	1.8	0.74	0.037	0.77	0.107	0.046	bdl	0.18	0.16	0.0015	0.00037	0.0016	0.039	0.00013
nv30a21.csv	208-37_FI-41	2.81	0.0008	2.0	0.43	0.027	0.58	0.016	0.025	0.00036	0.23	0.10	0.0004	0.00033	0.0014	0.022	0.00002
nv30a15.csv	208-37_FI-23	2.88	bdl	2.3	0.44	0.029	0.49	0.010	0.042	bdl	0.19	0.11	0.0002	0.00028	0.0007	0.040	0.00005
nv30a16.csv	208-37_FI-25	2.88	bdl	1.7	0.39	0.024	0.46	0.056	0.029	0.00022	0.16	0.11	0.0012	0.00020	0.0006	0.030	0.00005
nv30b14.csv	208-37_FI-18	2.88	0.0007	2.3	0.69	0.030	0.49	0.066	0.040	0.00032	0.20	0.10	0.0008	0.00032	0.0007	0.043	0.00008
nv30b16.csv	208-37_FI-22	3.17	bdl	1.7	0.39	0.023	0.46	0.060	0.029	0.00011	0.11	0.09	0.0014	0.00023	0.0008	0.033	0.00007
nv30b25.csv	208-37_FI-40	3.19	0.0007	2.3	0.59	0.024	0.47	0.013	0.026	0.00030	0.21	0.10	bdl	0.00030	0.0012	0.029	0.00002
nv30b21.csv	208-37_FI-34	3.75	0.0008	2.3	0.45	0.028	0.49	0.077	0.043	0.00048	0.11	0.08	0.0012	0.00027	0.0007	0.042	0.00009
nv30b20.csv	208-37_FI-33	3.97	0.0011	3.6	0.51	0.033	0.70	0.122	0.073	0.00052	0.20	0.12	0.0025	0.00033	0.0010	0.071	0.00017
nv30a17.csv	208-37_FI-27	4.04	0.0010	2.5	0.48	0.025	0.48	0.005	0.026	0.00033	0.21	0.06	0.0017	0.00030	0.0007	0.026	0.00003
nv30b24.csv	208-37_FI-39	4.19	bdl	3.6	0.45	0.025	0.53	0.006	0.038	0.00047	0.16	0.06	0.0005	0.00033	0.0009	0.039	0.00002
nv30b17.csv	208-37_FI-28	4.33	0.0006	2.1	0.43	0.019	0.37	0.012	0.023	0.00030	0.20	0.07	0.0004	0.00031	0.0002	0.027	0.00003
nv30b19.csv	208-37_FI-30	4.33	0.0007	2.4	0.47	0.025	0.50	0.086	0.040	0.00030	0.20	0.08	0.0017	0.00029	0.0010	0.046	0.00009
nv30b22.csv	208-37_FI-36	4.41	0.0005	2.2	0.34	0.021	0.42	0.052	0.038	0.00016	0.15	0.09	0.0014	0.00023	0.0006	0.041	0.00008
nv30b23.csv	208-37_FI-37	4.41	0.0005	2.2	0.35	0.024	0.48	0.062	0.041	0.00023	0.17	0.10	0.0013	0.00023	0.0007	0.040	0.00009
nv30b18.csv	208-37_FI-29	4.62	0.0006	2.0	0.39	0.024	0.52	0.053	0.037	0.00027	0.18	0.12	0.0014	0.00025	0.0008	0.036	0.00006
nv30b26.csv	208-37_FI-42	4.63	0.0006	2.2	0.25	0.024	0.48	0.068	0.039	0.00014	0.17	0.11	0.0014	0.00022	0.0007	0.040	0.00007
nv30a19.csv	208-37_FI-35	4.90	bdl	2.9	0.51	0.026	0.46	0.094	0.047	0.00045	0.07	0.07	0.0018	0.00031	0.0010	0.050	0.00010
nv30a27.csv	208-37_FI-52	5.11	0.0010	4.7	0.52	0.033	0.53	0.240	0.091	0.00055	0.30	0.09	0.0025	0.00040	0.0006	0.091	0.00017
nv30b27.csv	208-37_FI-44	5.74	0.0006	3.9	0.43	0.028	0.50	0.095	0.074	0.00040	0.20	0.10	0.0017	0.00032	0.0007	0.070	0.00013
nv30b28.csv	208-37_FI-46	5.96	bdl	5.1	0.51	0.032	0.55	0.140	0.083	0.00037	0.25	0.08	0.0020	0.00039	0.0007	0.087	0.00019
nv30b29.csv	208-37_FI-49	6.18	0.0017	5.5	0.50	0.035	0.64	0.095	0.089	bdl	0.16	0.05	0.0001	0.00044	0.0001	0.084	0.00017
nv30b30.csv	208-37_FI-47	6.18	0.0011	3.3	0.34	0.031	0.59	0.085	0.054	bdl	0.09	0.12	0.0010	0.00017	0.0009	0.052	0.00009
nv30a20.csv	208-37_FI-38	6.35	bdl	2.9	0.39	0.017	0.29	0.061	0.041	0.00030	0.18	0.06	0.0010	0.00027	0.0004	0.045	0.00009
nv30b31.csv	208-37_FI-51	6.62	0.0009	4.2	0.60	0.037	0.84	0.146	0.099	0.00024	0.24	0.16	0.0025	0.00040	0.0013	0.090	0.00019
		aspect ratio	B11	Cl35	K39	Mn55	Fe57	Cu65	Zn66	As75	Rb85	Sr88	Mo95	Cs133	Ba137	Pb208	Bi209
ja20a06.csv	Loww9 - FI 1	1.12	0.015	3.4	0.58	0.25	1.01	bdl	0.08	0.0001	0.027	0.034	0.0000024	0.034	0.00067	0.040	0.00013
ja20a09.csv	Loww9 - FI 4	1.28	0.014	3.1	0.63	0.25	1.02	0.0016	0.08	0.0015	0.021	0.038	bdl	0.031	0.00064	0.049	0.00019
ja20a10.csv	Loww9 - FI 5	1.44	0.012	2.9	0.42	0.19	0.75	0.0029	0.06	0.0013	0.019	0.026	bdl	0.026	0.00039	0.026	0.00015
ja20a07.csv	Loww9 - FI 2	1.54	0.012	3.2	0.60	0.23	0.88	0.0017	0.07	0.0012	0.024	0.033	bdl	0.030	0.00058	0.040	0.00015
ja20a12.csv	Loww9 - FI 6.2	1.64	0.012	2.8	0.54	0.19	0.72	0.0024	0.06	0.0010	0.020	0.025	bdl	0.025	0.00045	0.037	0.00014
ja20a14.csv	Loww9 - FI7	1.76	0.017	3.4	0.83	0.29	1.10	0.0027	0.08	0.0015	0.031	0.039	bdl	0.039	0.00070	0.053	0.00018
ja20a16.csv	Loww9 - FI9	1.76	0.018	3.8	0.90	0.31	1.22	0.0025	0.10	0.0017	0.034	0.040	0.0000015	0.044	0.00073	0.061	0.00023
ja20a17.csv	Loww9 - FI10	1.76	0.014	3.1	0.65	0.23	0.94	0.0028	0.07	0.0013	0.024	0.028	0.0000002	0.031	0.00055	0.042	0.00016
ja20a18.csv	Loww9 - FI11	1.91	0.011	2.7	0.54	0.18	0.68	0.0014	0.06	0.0006	0.020	0.023	bdl	0.026	0.00044	0.037	0.00013
ja20a15.csv	Loww9 - FI8	2.07	0.017	3.2	0.60	0.27	1.05	0.0030	0.08	0.0014	0.026	0.036	bdl	0.034	0.00072	0.050	0.00019
ja20a23.csv	Loww9 - FI12	2.07	0.020	4.0	0.88	0.33	1.25	0.0036	0.10	0.0003	0.031	0.042	bdl	0.039	0.00075	0.063	0.00023
ja20a32.csv	Loww9 - FI19	2.11	0.001	3.7	0.63	0.23	0.95	0.0021	0.09	0.0016	0.026	0.028	bdl	0.034	0.00060	0.054	0.00021
ja20a24.csv	Loww9 - FI13	2.23	0.015	3.4	0.69	0.25	1.00	0.0023	0.09	0.0015	0.026	0.034	0.0000014	0.033	0.00063	0.051	0.00019
ja20a11.csv	Loww9 - FI 6.1	2.23	0.011	3.0	0.62	0.20	0.81	0.0003	0.06	0.0012	0.022	0.024	0.0000013	0.028	0.00044	0.041	0.00009
ja20a33.csv	Loww9 - FI20	2.28	0.013	3.1	0.57	0.22	0.87	0.0014	0.07	0.0012	0.023	0.026	bdl	0.029	0.00051	0.042	0.00016
ja20a44.csv	Loww9 - FI27	2.87	0.014	3.5	0.66	0.23	0.92	0.0038	0.08	0.0014	0.025	0.027	bdl	0.034	0.00055	0.051	0.00021
ja20a25.csv	Loww9 - FI14	2.93	0.017	3.7	0.73	0.27	1.12	0.0026	0.09	0.0014	0.027	0.036	0.0000015	0.036	0.00069	0.054	0.00020
ja20a30.csv	Loww9 - FI17	3.05	0.019	3.9	0.69	0.26	1.04	0.0022	0.10	bdl	0.026	0.034	bdl	0.034	0.00065	0.061	0.00023
ja20a34.csv	Loww9 - FI21	3.28	0.014	3.3	0.57	0.21	0.83	0.0032	0.08	0.0012	0.021	0.027	bdl	0.028	0.00052	0.046	0.00018
ja20a38.csv	Loww9 - FI25	3.40	0.001	3.7	0.55	0.20	0.75	0.0032	0.08	0.0014	0.023	0.026	bdl	0.030	0.00055	0.050	0.00020
ja20a39.csv	Loww9 - FI26	3.52	0.020	4.1	0.64	0.20	0.81	0.0036	0.09	0.0016	0.024	0.023	bdl	0.031	0.00048	0.057	0.00022
ja20a45.csv	Loww9 - FI28	3.52	0.017	4.3	0.82	0.28	1.15	0.0044	0.12	0.0018	0.031	0.039	bdl	0.041	0.00066	0.071	0.00027
ja20a36.csv	Loww9 - FI23	3.75	0.016	3.5	0.59	0.21	0.83	0.0024	0.08	0.0014	0.022	0.025	bdl	0.029	0.00047	0.051	0.00020
ja20a47.csv	Loww9 - FI30	4.10	0.018	4.1	0.79	0.26	1.00	0.0029	0.09	0.0014	0.030	0.032	bdl	0.040	0.00063	0.058	0.00022
ja20a27.csv	Loww9 - FI16.3	4.15	0.022	4.5	0.84	0.32	1.04	0.0037	0.13	0.0024	0.038	0.045	0.0000040	0.050	0.00076	0.081	0.00030
ja20a28.csv	Loww9 - FI16.2	4.15	0.018	4.4	0.81	0.29	1.18	0.0023	0.09	0.0018	0.032	0.039	bdl	0.042	0.00077	0.061	0.00024
ja20a29.csv	Loww9 - FI16.3	4.15	0.029	5.7	1.03	0.36	1.23	0.0047	0.15	0.0029	0.045	0.043	bdl	0.057	0.00084	0.090	0.00040
ja20a35.csv	Loww9 - FI22	4.31	0.014	3.5	0.51	0.16	0.65	0.0010	0.08	0.0001	0.021	0.019	bdl	0.027	0.00039	0.049	0.00014
ja20a53.csv	Loww9 - FI36	4.34	0.013	3.9	0.64	0.22	0.84	0.0024	0.09	0.0003	0.025	0.027	bdl	0.032	0.00049	0.054	0.00021
ja20a37.csv	Loww9 - FI24	4.47	0.014	3.8	0.77	0.25	1.00	0.0029	0.08	0.0015	0.029	0.036	bdl	0.038	0.00069	0.055	0.00022
ja20a55.csv	Loww9 - FI39	4.55	0.015	3.8	0.65	0.21	0.83	0.0027	0.08	0.0015	0.026	0.025	bdl	0.033	0.00049	0.052	0.00020

References:

1. J. Ihlemann, *Applied Surface Science*, 1992, **54**, 193-200.
2. I. Horn, M. Guillong and D. Gunther, *Applied Surface Science*, 2001, **182**, 91-102.